Measurement of iron cosmic-ray primaries below 10GeV/n by use of the geomagnetic effect with CALET

M.Ichimura[a] and K.Kasahara[b] for the CALET collaboration

[a] *Faculty of Science and Technology, Graduate School of Science and Technology, Hirosaki University, 3, Bunkyo, Hirosaki, Aomori 036-8561, Japan*

[b] *Department of Electronic Information Systems, Shibaura Institute of Technology, 307 Fukasaku, Minuma, Saitama 337-8570, Japan*

Abstract

The CALET Calorimeter on the International Space Station(ISS) has previously measured the flux and spectrum of iron cosmic-ray nuclei above 10 GeV/n. In order to extend the measurement to the region below 10 GeV/n, we carry out an analysis to utilize the geomagnetic effect. Cutoff rigidities of cosmic-ray nuclei are calculated for all directions for each observation point in the ISS orbit. The integral spectrum of observed rigidities is then obtained by counting the number of iron nuclei in each bin of cutoff rigidity. The absolute flux and differential spectrum are then calculated by taking the detection efficiencies into account. Here we present the details of the analysis procedure and the iron spectrum below 10 GeV/n.

CALET instrument

The CALET calorimeter consists of three parts. The upper part, the CHarge Detector (CHD), is composed of two layers of 1 cm thick plastic scintillators, CHDx and CHDy. It is used for the charge determination of the incident particles. Below that, the Imaging Calorimeter (IMC) is installed. It consists of 448 scintillating fibers with a cross-section of 1 mm by 1 mm, stacked one layer each in the orthogonal x and y directions, alternating with tungsten plates. It is used for track reconstruction and the detailed study of shower development. The lower part is the Total AbSorption Calorimeter (TASC), which is composed of twelve layers of 2 cm thick PWO scintillators stacked in the x and y directions. It is used for energy determination. Details on the instrument can be found in the Supplemental Material (SM) of Ref. [1]. In this study, only the CHD and IMC were used for the analysis.

Calculation of cutoff rigidity by the backtracing method

Cutoff rigidity calculations were performed for every direction at observation points along the ISS orbit.

Calculation of the geomagnetic field at a fixed time

The calculation is performed by the two geomagnetic field models together, IGRF13(International Geomagnetic Reference Field)[2] and TS05[3]. IGRF is a standard model for the internal magnetic field. TS05 is a model for the external magnetic field with the disturbance caused by the solar wind.

Backtracing

The latitude, longitude, and altitude of the observation point are set, and an antiproton is emitted in the direction of a certain zenith angle and a certain azimuthal angle with a certain rigidity R. Then, while solving the motion equations using the Runge-Kutta method, the particle track is traced. Tracing will be stopped when; 1) the particle hit the earth, 2) the particle reaches the magnetopause, and 3) the particle is far from the earth more than 15 times the earth's radius. In case (1), this condition is classified in the forbidden region. A nucleus cannot enter from this direction with this rigidity. In cases (2) and (3), these conditions are classified in the allowed region. A nucleus can enter from this direction with this rigidity.

Cutoff Rigidity calculation

The backtracing calculation for one direction is repeated by varying the rigidity from 1 GV to 50 GV with the step of 0.01 in a logarithmic scale. In the results of this calculation, we can observe the alternating appearance of the forbidden region and allowed region which is known as the penumbra region. Effective cutoff Rigidity, Rc, is calculated by compressing the penumbra structure by the method described in Ref. [4]. This Rc is adopted as the final cutoff rigidity.

The cutoff Rigidity dome calculation (Rc dome)

At each observation point, the above calculation is performed for all zenith angles and azimuthal angles, and the cutoff rigidity dome (Rc dome) is calculated as shown in Fig. 1.

- The azimuthal direction is divided into 24 bins at 15-degree intervals.
- The zenith angle direction is divided into to 6 parts with equal steps in the scale of cos $\theta d(\cos\theta)$.
- Rc calculations are done by backtracing for each solid angle bin.

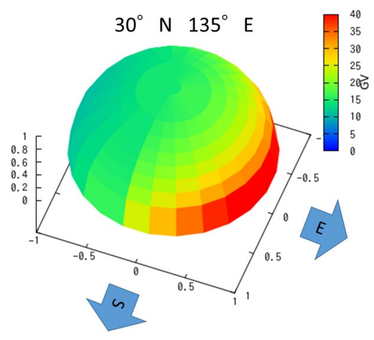

Figure 1: Rc dome at LAT 30N LON 135E. The colors represent the values of Rc.

In this analysis, the region within a zenith angle of 45 degrees was used.

The calculation of such Rc domes was performed for each observation point along the ISS orbit The analysis period is 68 months from October 2015 to May 2021, and the UH trigger mode[5] periods have been picked up. The total number of observation points considered in the calculation was about 25,000 points per month.

Charge Determination

Charge determination has been done by the CHDx and CHDy signals. The CHD signals are expected to depend on rigidity, so we divided the Rc range from $10^{0.50}$ GV to $10^{1.30}$ GV into 16 equal parts on a log scale. Additionally, tracks with rigidity greater than $10^{1.30}$ GV(19.95 GV) were grouped as the 17th bin. The following charge determination process was done for each Rc bin.

First, a cross-plot of the CHDx and CHDy signals with zenith angle correction was made for the picked-up tracks as shown in Fig. 2(a). Figure 2 shows the plots for all tracks without Rc binning for reference. Tracks with a difference between CHDx and CHDy within 10% were selected (Fig. 2(b)), and histograms were generated for CHDx and CHDy respectively. Fig. 2(c) shows the histogram for CHDx.

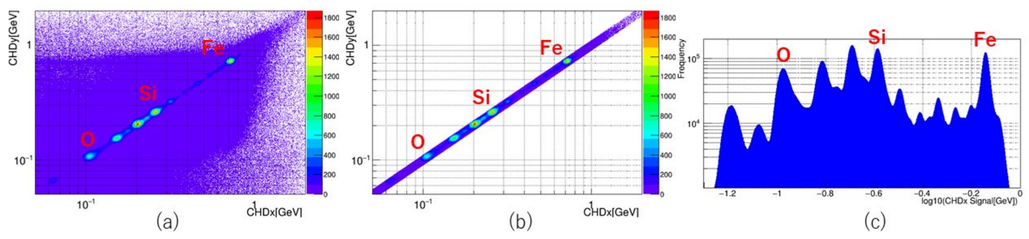

Figure 2: For all tracks triggered by the UH trigger; (a) the CHDy signal vs the CHDx signal. There are some clusters corresponding to the major component of cosmic ray nuclei. (b) The tracks with CHDx and CHDy signals are within 10% of each other. (c) The histogram of the CHDx signal for the tracks in the plot (b). The horizontal axis shows log10(CHDx).

We can read the peak value of the CHD histogram for each nucleus component. For the conversion of the peak value to charge, the relationship between the CHD signal and the atomic number squared (z^2) were fitted using the halo model [6]. Using this model, estimated charges (Zx, Zy) corresponding to CHDx and CHDy were calculated for each Rc bin. Figure 3 shows the standard deviation for Zx and Zy for each Rc bin. One can see that σ_{Zy} is greater than σ_{Zx} for all Rc bins. The tracks with both Zx and Zy within 26 $\pm 1.2\sigma$ are adopted as candidates for iron nuclei.

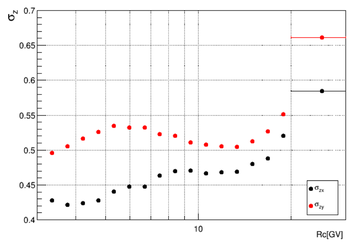

Figure 3: The standard deviation for the estimated charges by CHDx and CHDy. The horizontal axis shows Rc values. Points correspond to each of the 17 Rc bins. The last bin represents the Rc range greater than 19.95 GV.

Calculation of the flux

For the adopted iron nucleus candidates, they can be associated with Rc for each observation point and incident direction that was calculated beforehand. By counting the number of iron nuclei in each Rc bin and simultaneously using the number of solid angle bins and the sum of live time for the corresponding Rc bin, an integrated rigidity spectrum was calculated. The results are shown in Fig. 4. The different colors represent different ranges of zenith angles. This spectrum was converted to a differential spectrum as shown in Fig. 5.

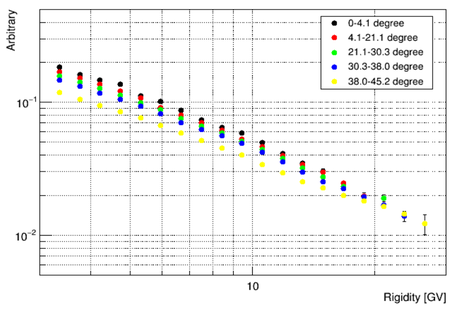

Figure 4: The integral rigidity spectrum of iron nuclei. It is obtained by counting the number of iron nuclei for each Rc bin and dividing by solid angle times observation time. The colors represent different ranges of zenith angles.

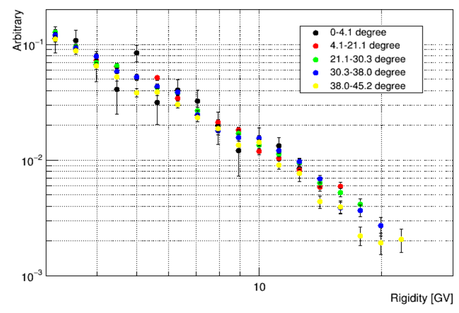

Figure 5: The Differential rigidity spectrum of iron nuclei converted from Fig. 4.

Detection efficiency

For the absolute flux, geometric and tracking efficiencies were calculated by the Cosmos8.042 + Epics9.311 simulation code[7, 8]. Two different Interaction models, the phits [9] and the jam[10], are used for this calculation for different energy regions. Iron nuclei were incident on the CALET detector, and the efficiency was calculated using the same condition as the observation data. The results are shown in Fig. 6. The horizontal axis represents the kinetic energy per particle and the colors represent different ranges of zenith angles. Larger zenith angles have more interaction, so the efficiency becomes lower.

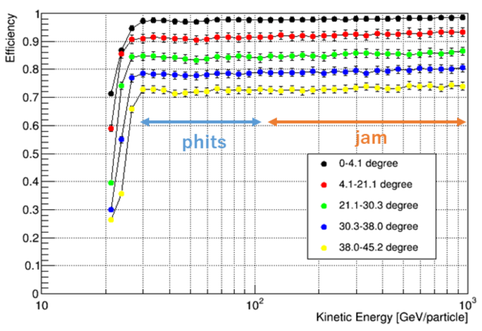

Figure 6: Tracking and geometrical efficiency of iron nuclei.

Systematic uncertainties

The following systematics are estimated by the simulation calculation and by the observation data.

- fluctuation of flux due to the precision of cutoff rigidity determination:
  - The influence of bin width in longitude and latitude : about 8%
  - The variation of Rc within the solid angle bin : about 5%
- The effect of the charge identification cut : less than 2%. Furthermore, for
- The longterm stability: about 10%.

At this stage, the systematic uncertainty due to the interaction model is not considered yet.

Absolute flux

Figure 7 shows the rigidity spectrum of the iron nuclei obtained by this work. The detection efficiencies were taken into account for each zenith angle range, then combined in one spectrum. The vertical axis represents the differential absolute flux. The error bars show the statistical errors and the colored band indicates the quadrature sum of statistical and systematic errors which are mentioned above. Flux has been calculated from 3 GV to more than 20 GV. It seems that the rigidity spectrum follows a single power law with a power index of about -2.0.

The energy spectrum with kinetic energy per nucleon from 1 GeV/n to 10 GeV/n is shown in Fig. 8. The vertical axis represents the flux multiplied by $E^{2.6}$.

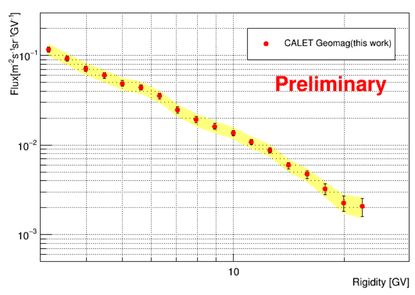

Figure 7: The rigidity spectrum of the absolute flux for iron nuclei. The error bars show the statistical errors and the colored band indicates the quadrature sum of statistical and systematic errors.

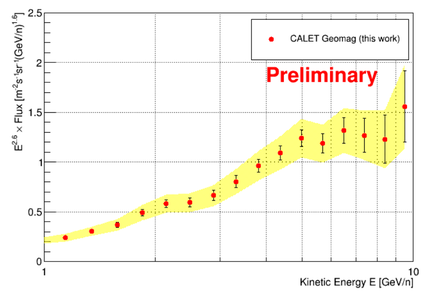

Figure 8: The energy spectrum of the absolute flux for iron nuclei. The horizontal axis shows the kinetic energy per nucleon. The error bars show the statistical errors and the yellow zone indicates the quadrature sum of statistical and systematic errors.

In this analysis, only the events with a zenith angle within 45 degrees were analyzed using a limited period of observations until May 2021. However, by including tracks with larger zenith angles in the analysis, it is possible to increase the statistics up to larger values of Rc and extend the spectrum towards higher rigidities.

In this energy range, the flux undergoes significant variations due to solar modulation. To compare our results with other observations, it is necessary to quantitatively evaluate the solar modulation effect for each observation period. This will be future work.

References

[1] O. Adriani et al.(CALET Collaboration), *Phys.Rev.Lett.*, 119,181101(2017).
[2] P. Alken et al., *Earth Planets Space*, 73, 49(2021).
[3] N.A. Tsyganenko and M.I. Sitnov, *J. Geophys. Res.*, 110, A03208(2005).
[4] E. Kamioka et al., *Astroparticle Physics*, 6, 155(1997).
[5] A.W. Ficklin, N. Cannady, B.F. Rauch and W. Zober(CALET), *Pos(ICRC2021)*, 069(2021).
[6] P.S. Marrocchesi et al., *NIM*, A659, 477(2011).
[7] E. Kamioka et al., *Astroparticle Physics*, 6, 155(1997).
[8] See EPICS webpage http://cosmos.n.kanagawa-u.ac.jp/EPICSHome/
[9] K. Niita et al., *Radiation Measurements*, 41, 1080(2006).
[10] Y. Nara et al., *Phys.Rev.C*, 61, 024901(1999).

Acknowledgments

We gratefully acknowledge JAXA's contributions to the development of CALET and the operations onboard the International Space Station. The CALET effort in Italy is supported by ASI under Agreement No. 2013- 018-R.0 and its amendments. The CALET effort in the United States is supported by NASA through Grants No. 80NSSC20K0397, No. 80NSSC20K0399, and No. NNH18ZDA001N-APRA18-0004. This work is supported in part by JSPS Grant-in-Aid for Scientific Research (S) Grant No. 19H05608 and (C) Grant No. 20K03982 in Japan.